LETTERS
PUBLISHED ONLINE: 13 JULY 2014 | DOI: 10.1038/NPHYS3021

nature physics

Underdoped superconducting cuprates as topological superconductors

Yuan-Ming Lu[1,2], Tao Xiang[3] and Dung-Hai Lee[1,2]*

Superconductivity in copper oxide (cuprate) high-transition-temperature superconductors follows from the chemical doping of an antiferromagnetic insulating state. The consensus that the wavefunction of the superconducting carrier, the Cooper pair, has $d_{x^2-y^2}$ symmetry[1,2] has long been reached. This pairing symmetry implies the existence of nodes in the superconducting energy gap. Recently, a series of angle-resolved photoemission spectroscopy experiments[3–9] have revealed that deeply underdoped cuprates exhibit a particle–hole symmetric[3] superconducting-like energy gap at the momentum-space locations where the $d_{x^2-y^2}$ gap nodes are expected. Here we discuss the possibility that this phenomenon is caused by a fully gapped topological superconducting state that coexists with the antiferromagnetic order. If experimentally confirmed, this result will completely change our view of how exactly the high-temperature superconductivity state evolves from the insulating antiferromagnet.

Topological arguments[10–13] have been put forward to understand the robustness of the $d_{x^2-y^2}$ gap nodes in the cuprates. Therefore it was a surprise when the 'nodal gap' was experimentally observed for $Bi_2Sr_2CaCu_2O_{8+\delta}$ (Bi2212; refs 4,5), $La_{2-x}Sr_xCuO_4$ (LSCO; refs 6, 7,9), $Bi_2Sr_{2-x}La_xCuO_{6+\delta}$ (Bi2201; ref. 3) and $Ca_{2-x}Na_xCuO_2Cl_2$ (NaCCOC; ref. 8). The magnetic and transport properties of the systems manifest a nodal gap range from 'weak' antiferromagnetic (AF) insulators[3,7] to superconductors[5,7]. For example, in Bi2212, a phase diagram with a new superconducting (SC) phase appearing at the underdoped end of the SC dome has been proposed[5]. In contrast the samples showing the 'nodal gap' in ref. 3 are insulating and antiferromagnetic. However, despite these differences, relatively sharp coherence peaks were observed at the nodal gap edge in both cases[3,5]. On the basis of this fact, refs 3,5 concluded that it is unlikely that such a gap is caused by disorder. However, given the fact that samples at such a low doping level can have strong phase inhomogeneity[14], we interpret the sharp coherence peaks[3] as coming from poorly connected SC islands embedded in an insulating background.

In the literature, proposals for the origin of the nodal gap range from a disorder-induced Coulomb gap[15] to spectral weight transfer due to the polaron effect[3]. However, as pointed out in refs 3,5 in both of the above scenarios one does not expect sharp coherence peaks. Motivated by refs 3,5,7 we assert that the state responsible for the nodal gap is a fully gapped SC state. Moreover, because samples exhibiting the nodal gap are found at the border between AF and SC phases we consider the possibility that such a SC state coexists with the AF order.

In the rest of the paper we first tabulate all possible fully gapped SC states and organize them into different symmetry-protected topological classes (Table 1). We then perform explicit calculations, using the AF exchange as the effective interaction, to determine the leading and subleading SC instabilities. The combination of these two approaches allows us to pin down the most likely state responsible for the nodal gap—namely, a spinful $p+ip$ topological SC state.

Starting with the maximum possible symmetry of a SC state, we systematically break down the $SU(2)_{spin} \times \boldsymbol{T}$ symmetry ($\boldsymbol{T}$ for time reversal). For each residual symmetry we use the method of refs 16, 17 to classify the possible fully gapped SC states into topological classes. Because cuprates are quasi-two-dimensional materials we restrict ourselves to two space dimensions. The result is shown in Table 1, where each row represents a symmetry class. We group these classes according to whether superconductivity coexists with AF order or not. In view of the fact that the samples are probably disordered we do not consider crystal translation symmetry. However, we do regard the system as having inversion symmetry, at least on average, so that even- and odd-parity pairing do not mix. Near the end we will discuss the effects of inversion symmetry breaking.

In the absence of Néel order there is spin SU(2) symmetry (in this paper we neglect spin–orbit interactions, which is a good approximation for the cuprates). In the singlet pairing case there are two classes of fully gapped SC states: the s-wave pairing (row 2) and $d \pm id$ pairing (row 3). The latter is a topological SC state with chiral (complex) fermion edge modes. In fact, in ref. 7 $d \pm id$ was proposed as an explanation for the nodal gap in LSCO. In the triplet pairing case there are three classes of fully gapped SC states. They are listed in rows 4–6 of Table 1. The $(p \pm ip)_{\uparrow\downarrow}$ SC state in the fourth row breaks time-reversal symmetry but preserves U(1) spin rotation around, say, the z-axis. It is a representative of a family of degenerate triplet pairing states given by $\cos\theta(p \pm ip)_{\uparrow\downarrow} + \sin\theta e^{-i\phi}(p \pm ip)_{\uparrow\uparrow} + \sin\theta e^{i\phi}(p \pm ip)_{\downarrow\downarrow}$, where $\vec{d} = (\sin\theta\cos\phi, \sin\theta\sin\phi, \cos\theta)$ is the direction of the axis around which the $U(1)_{spin}$ symmetry is preserved. The SC states in this class possess chiral (complex) fermion edge modes and, hence, are topologically non-trivial. In row 5 the $(p \pm ip)_{\uparrow\uparrow} + (p \mp ip)_{\downarrow\downarrow}$ SC state preserves time-reversal symmetry but completely breaks spin SU(2) symmetry. It has a pair of counter-propagating Majorana modes along each edge. The SC state in the row 6 of Table 1 has no residual symmetry. The SC state possesses two chiral Majorana (equivalent to one complex) fermion edge modes. Hence they, too, are chiral topological superconductors.

The cases where the fully gapped SC state coexists with Néel order are listed in the last three rows of Table 1. Here, without loss of generality, we can assume the staggered magnetic moments point in the $\pm z$-direction. The pairing states in row 7 are all topologically trivial—they are exemplified by the s-wave pairing. In contrast the $d \pm id$ and the $(p \pm ip)_{\uparrow\downarrow}$ SC states in the row 8 both give rise to chiral topological superconductors with chiral (complex) fermion edge modes. We note that the residual symmetry

[1]Department of Physics, University of California, Berkeley, California 94720, USA, [2]Materials Sciences Division, Lawrence Berkeley National Laboratory, Berkeley, California 94720, USA, [3]Institute of Physics, Chinese Academy of Sciences, Beijing 100190, China. *e-mail: dunghai@berkeley.edu

© 2014 Macmillan Publishers Limited. All rights reserved

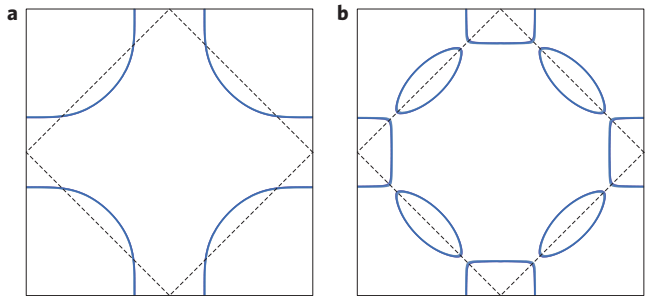

Figure 1 | The Fermi surface of cuprates without and with antiferromagnetic (AF) order. The thin dashed diamond encloses the AF Brillouin zone whose vertices are $(\pm\pi/a, 0)$ and $(0, \pm\pi/a)$. **a**, Fermi surface without AF order. **b**, Fermi surface with AF order. The staggered moment used to construct panel **b** is $m = 0.1$.

of the $(p \pm \mathrm{i}\, p)_{\uparrow\downarrow}$ superconductor in row 8 is exactly the same as that in row 4. However, unlike row 4, there is no longer continuous degeneracy because the $\mathrm{SU}(2)_{\mathrm{spin}}$ is already broken down to $\mathrm{U}(1)_{\mathrm{spin}}$ by the formation of the Néel order. The SC states in the row 9 are analogous to that given in the row 6, and are topologically non-trivial.

Having listed all possible fully gapped SC states, we next determine to which symmetry class of Table 1 the experimentally observed fully gapped SC state belongs. To achieve that we use the following effective Hamiltonian introduced in ref. 18

$$H_{\mathrm{eff}} = \sum_{\mathbf{k}}{}' \sum_{\sigma} \epsilon(\mathbf{k}) \psi^{+}_{\sigma\mathbf{k}} \psi_{\sigma\mathbf{k}} + J \sum_{\langle i,j \rangle} \mathbf{S}_i \cdot \mathbf{S}_j \qquad (1)$$

to predict the leading and subleading SC instabilities in the presence/absence of AF order. (See Supplementary Information for details on the band structure parameters and, in the case of AF state, the value of staggered magnetization.) In equation (1) $\sum_{\mathbf{k}}{}'$ stands for sum within a thin shell around the Fermi surface and $\psi_{\sigma\mathbf{k}}$ annihilates an electron with spin σ and momentum $\mathbf{k}$ within the momentum shell. $\mathbf{S}_i$ is the real space electron spin operator. It is transformed into the appropriate form in the band eigenbasis in the actual calculation.

Examples of the normal state Fermi surface with and without AF order are shown in Fig. 1. The Fermi pockets centred along the Brillouin zone diagonal are the hole pockets, whereas those centred at the Brillouin zone faces are electron pockets. Based on equation (1) and the above bandstructure we fix a low temperature, decouple the AF interaction in all possible pairing channels, and determine the gap functions that will first (and second) become unstable as J is turned up from zero. (See the Supplementary Information for more details.)

Cooper pairing in the absence of AF order

Figure 2a,b illustrates all SC instabilities in the absence of AF order[18]. The leading instability (panel (a)) occurs in the $d_{x^2-y^2}$ channel, which has four nodes and, hence, can not be responsible for the fully gapped state observed in experiments. The subleading instability occurs in the extended s-wave channel. However, it has an approximate $\cos k_x + \cos k_y$ symmetry (due to the nearest neighbour AF interaction) which also possesses nodes and, hence, does not give rise to a fully gapped SC state. One might argue that these nodes are not protected by symmetry and, hence, can be absent in the presence of disorder. However, for systems with pure repulsive interaction, such as the cuprates, a nodeless s-wave superconducting state is not energetically favourable. Thus rows 2–6 of Table 1 are ruled out on the basis that at least one component (for example, the d_{xy} of $d_{x^2-y^2} + \mathrm{i}\, d_{xy}$) of the gap function is not among the pairing instabilities in Fig. 2a,b.

Cooper pairing in the presence of AF order

In the presence of AF order, the symmetry of the superconducting gap function is labelled by the parity and the S_z eigenvalues. The leading and subleading pairing instabilities both occur in the $S_z = 0$ channel and are shown in Fig. 2c–e. The leading paring symmetry is even parity, $S_z = 0$, and transforms like $d_{x^2-y^2}$ under rotation. It possesses nodes hence can not account for the presence of nodal gap. The subleading gap functions, are doubly degenerate. They have odd parity, $S_z = 0$ and transform under rotation like p_{x+y} and p_{x-y} (Fig. 2d,e). Although they each have nodes, the linear combination $(p \pm \mathrm{i}\, p)_{\uparrow\downarrow}$ (the spin subscript emphasizes the $S_z = 0$ nature of the pairing) can give rise to a fully gapped superconductor. This superconductor belongs to the topological class of row 8 of Table 1, is chiral and possesses complex fermion edge modes. Therefore, combining Table 1 with explicit calculations, we conclude that the best candidate for the experimentally observed fully gapped state is the $(p \pm \mathrm{i}p)_{\uparrow\downarrow}$ SC coexisting with AF order.

According to refs 3,5,7 the nodal gap magnitude increases as $\mathbf{k}$ moves away from the diagonal direction. This is qualitatively consistent with the behaviour of $|\Delta_d(\mathbf{k}) + \mathrm{i}\, \Delta_e(\mathbf{k})|$ (Fig. 2f), where $\Delta_{d,e}(\mathbf{k})$ are the gap functions of Fig. 2d,e. In Fig. 3 we show the edge spectrum of the SC state discussed above. Explicit wavefunction calculations show the left/right-moving in-gap modes are localized on opposite edges. However, despite the presence of edge states, we do not expect the superconducting vortex to harbour zero modes.

Table 1 | Symmetry and topological classification of fully gapped superconducting phases in two spatial dimensions.

Néel order	Symmetry	Generators	Classification	AZ class	Examples
No	$\mathrm{SU}(2)_{\mathrm{spin}} \times \boldsymbol{T}$	$\boldsymbol{T}\{e^{\mathrm{i}\pi S_x}, e^{\mathrm{i}\pi S_y}, e^{\mathrm{i}\pi S_z}\}$	$\pi_0(R_5) = 0$	CI	s-wave
No	$\mathrm{SU}(2)_{\mathrm{spin}}$	$\{e^{\mathrm{i}\pi S_x}, e^{\mathrm{i}\pi S_y}\}$	$\pi_0(R_4) = \mathbb{Z}$	C	$d \pm \mathrm{i}d$
No	$\mathrm{U}(1)_{\mathrm{spin}}$	$\{e^{\mathrm{i}\pi S_z}\}$	$\pi_0(C_2) = \mathbb{Z}$	A	$(p \pm \mathrm{i}p)_{\uparrow\downarrow}$
No	$\boldsymbol{T}$	$\boldsymbol{T}$	$\pi_0(R_1) = \mathbb{Z}_2$	DIII	$(p \pm \mathrm{i}p)_{\uparrow\uparrow} + (p \mp \mathrm{i}p)_{\downarrow\downarrow}$
No	None	N/A	$\pi_0(R_0) = \mathbb{Z}$	D	$\alpha(p \pm \mathrm{i}p)_{\uparrow\uparrow} + \beta(p \pm \eta \mathrm{i}p)_{\downarrow\downarrow}$
Yes	$\mathrm{U}(1)_{S_z} \times \boldsymbol{T} e^{\mathrm{i}\pi S_x}$	$\boldsymbol{T}\{e^{\mathrm{i}\pi S_x}, e^{\mathrm{i}\pi S_y}\}$	$\pi_0(R_6) = 0$	AI	s-wave
Yes	$\mathrm{U}(1)_{S_z}$	$\{e^{\mathrm{i}\pi S_z}\}$	$\pi_0(C_2) = \mathbb{Z}$	A	$(d \pm \mathrm{i}d)\,;\,(p \pm \mathrm{i}p)_{\uparrow\downarrow}$
Yes	None	N/A	$\pi_0(R_0) = \mathbb{Z}$	D	$\alpha(p \pm \mathrm{i}p)_{\uparrow\uparrow} + \beta(p \pm \eta \mathrm{i}p)_{\downarrow\downarrow}$

We assume there is no spin–orbit interaction. The second column lists the symmetry group whose generators are given in the third column. The fourth column gives the Abelian group whose elements each represent a topological class of superconducting states[17,19] (for details see supplementary Methods). 0 means no topological superconductors, $\mathbb{Z}_2$ means there exists one type of topological superconductor in addition to the trivial superconductor. $\mathbb{Z}$ represents the existence of an infinite number of different topological superconductors, each with protected gapless edge modes. The fifth column locates the symmetry class of each row in the Altland–Zirnbauer[20] ten-fold way[16,17]. The last column provides examples of gapped superconducting states in each symmetry class. Here $(p + \mathrm{i}p)_{\uparrow\downarrow}$ denotes the $p + \mathrm{i}p$ pairing between the spin-up and spin-down electrons, and $(p + \mathrm{i}p)_{\uparrow\uparrow}, (p + \mathrm{i}p)_{\downarrow\downarrow}$ represents $p + \mathrm{i}p$ pairing between spin-up and/or spin-down electrons. In row 6 and 9, α and β denote generic complex numbers while $\eta = \pm 1$.

© 2014 Macmillan Publishers Limited. All rights reserved

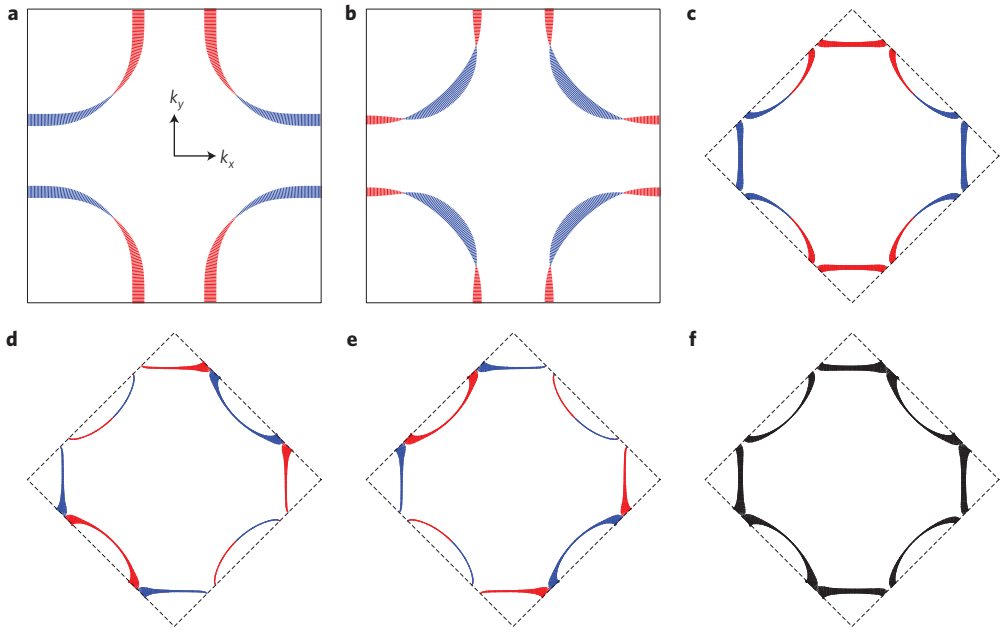

Figure 2 | The superconducting instabilities of equation (1). a,**b**, Leading and subleading superconducting instabilities in the absence of Néel order. **c**–**e**, Leading and subleading superconducting instabilities in the presence of Néel order. Singlet $d_{x^2-y^2}$ symmetry (**a**), extended *s* symmetry (**b**), even parity $d_{x^2-y^2}$ symmetry (**c**), odd parity p_{x+y} symmetry (**d**) and odd parity p_{x-y} symmetry (**e**). In **a**–**e** the hatch size is proportional to the magnitude of the gap and the colour indicates the sign (red: negative, blue: positive). **f**, Energy gap corresponding to $|\Delta_d(\mathbf{k})+\mathrm{i}\,\Delta_e(\mathbf{k})|$. Here black means positive and the hatch size is proportional to the gap magnitude.

This is because in one dimension (the dimension of a loop encircling the vortex) the symmetry class of row 8 of Table 1 has only trivial states (Supplementary Information).

Discussion

A natural question one might ask is why odd-parity pairing instability exists in the AF state but not in the paramagnetic state. Here we provide a physical picture. In the presence of AF order, the conserved spin quantum number is S_z and Cooper pair with centre-of-mass momentum $(0,0)$ and (π,π) can be mixed. For simplicity let us consider three adjacent sites, labelled by $i-1, i, i+1$ in, say, the x-direction of the square lattice. The Cooper pair operator

$$\alpha[(c_{i-1\uparrow}c_{i\downarrow}-c_{i-1\downarrow}c_{i\uparrow})+(c_{i\uparrow}c_{i+1\downarrow}-c_{i\downarrow}c_{i+1\uparrow})] +\beta[(c_{i-1\uparrow}c_{i\downarrow}+c_{i-1\downarrow}c_{i\uparrow})-(c_{i\uparrow}c_{i+1\downarrow}+c_{i\downarrow}c_{i+1\uparrow})] \quad (2)$$

is a linear combination of momentum (0,0) singlet pairing and momentum (π,π) triplet pairing. On inversion around i (that is, $i-1\leftrightarrow i+1$) it has even parity. Similarly the Cooper pair operator

$$\alpha'[(c_{i-1\uparrow}c_{i\downarrow}-c_{i-1\downarrow}c_{i\uparrow})-(c_{i\uparrow}c_{i+1\downarrow}-c_{i\downarrow}c_{i+1\uparrow})] +\beta'[(c_{i-1\uparrow}c_{i\downarrow}+c_{i-1\downarrow}c_{i\uparrow})+(c_{i\uparrow}c_{i+1\downarrow}+c_{i\downarrow}c_{i+1\uparrow})] \quad (3)$$

is a linear combination of momentum (0,0) triplet and momentum (π,π) singlet and has odd parity. In equations (2) and (3) $c_{i,\uparrow}$ and $c_{i,\downarrow}$ annihilate a spin up and down electron on site i, and $\alpha,\beta,\alpha',\beta'$ are complex numbers. Notice that both operators contains a bond singlet component, which is favoured by the nearest neighbour AF interaction. One might also ask 'under what condition will the odd-parity pairing in Fig. 2d,e become the leading instability?' It turns out that this can be achieved in a number of ways, such as increasing the staggered moment m (because a larger moment causes stronger mixing between the singlet momentum $(\pi,\pi)/(0,0)$ and triplet momentum $(0,0)/(\pi,\pi)$ channels), slightly modifying the bandstructure such that in the AF state there are only hole pockets, or adding a nearest neighbour repulsion to the effective interaction. For example, by using $t_1=1, t_2=0.3, t_3=0.1$, $\mu=0.25$, $m=0.3$, where the Fermi surface in the AF state consists of hole pockets only, the two degenerate odd-parity gap functions become the leading SC instability. This result is shown in the Supplementary Information. Next we comment on the effects of inversion symmetry breaking. Without inversion symmetry even-parity (Fig. 2c) and odd-parity (Fig. 2d,e) pairing can mix. This can be induced by disorder or phase inhomogeneity. We have checked that the superconductor with $\alpha d_{x^2-y^2}+\beta(p\pm\mathrm{i}\,p)_{\uparrow\downarrow}$ can be fully gapped. Furthermore, there is a wide range of $|\alpha/\beta|$ in which edge states persist. The temperature dependence of the nodal gap is another important issue. In our picture the nodal gap, which signifies the $p+ip$ pairing, should close at a relatively low temperature. Experimentally, the ARPES spectra consist of two kinds of gap: a large smooth pseudogap (arising from both the insulating and superconducting regions) and a relatively sharp small gap which exists in the $p+\mathrm{i}\,p$ superconducting region only. The pseudogap survives to very high temperatures whereas the much smaller $p+\mathrm{i}\,p$ superconducting gap does not. Because of the different temperature dependence of the two gaps, determining the temperature dependence of the superconducting gap is a very delicate matter. Nonetheless, a recent result in deeply underdoped LSCO shows that the nodal gap vanishes at temperature ~40 K (ref. 9). Given the fact that AF order induces odd-parity pairing instability, an interesting question arises: Is it possible that strong fluctuations of the Néel order parameter (which should exist near the AF–SC boundary) can stabilize the odd-parity topological SC order even when there is no static AF order?

In conclusion we propose that deeply underdoped cuprates can be a topological superconductor. One way to experimentally test our prediction is to use STM to image the edge states. Another method is to detect a signature of the chiral superconductivity,

© 2014 Macmillan Publishers Limited. All rights reserved

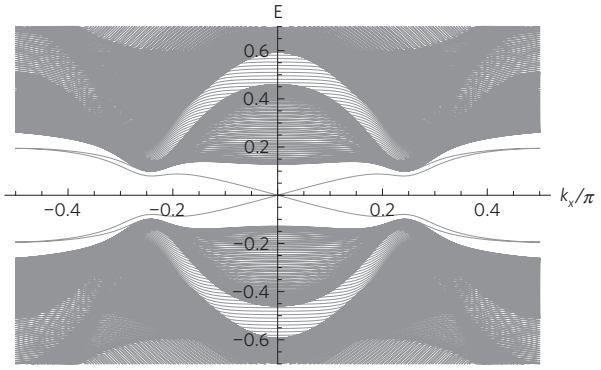

Figure 3 | Edge spectrum of the $(p+ip)_{\uparrow\downarrow}$-AF coexisting state. As a result of the Brillouin zone folding $k_x = -\pi/2$ and $k_x = \pi/2$ are equivalent. The left/right-moving branches are localized on opposite edges. This figure is constructed by fitting the numerical gap functions in Fig. 2d,e to simple trigonometric functions, then using the fitted function in the real space edge calculation. Here the direction k_x is that indicated in Fig. 2a.

such as the change in the amount of Kerr rotation. Given the likelihood that the sample is phase separated, STM is a particularly valuable probe for the signature of the topological superconductivity locally. Finally, we note that although the discussion is tailored to the cuprates, the physics discussed here can apply to other materials exhibiting the coexistence of antiferromagnetism and superconductivity. Candidate systems include the heavy-fermion superconductors, or even the iron-based superconductors.

Received 2 March 2014; accepted 11 June 2014;
published online 13 July 2014

References

1. Van Harlingen, D. J. Phase-sensitive tests of the symmetry of the pairing state in the high-temperature superconductors—evidence for $d_{x^2-y^2}$ symmetry. *Rev. Mod. Phys.* **67,** 515–535 (1995).
2. Tsuei, C. C. & Kirtley, J. R. Pairing symmetry in cuprate superconductors. *Rev. Mod. Phys.* **72,** 969–1016 (2000).
3. Peng, Y. *et al.* Disappearance of nodal gap across the insulator–superconductor transition in a copper-oxide superconductor. *Nature Commun.* **4,** 2459 (2013).
4. Tanaka, K. *et al.* Distinct Fermi-momentum-dependent energy gaps in deeply underdoped Bi2212. *Science* **314,** 1910–1913 (2006).
5. Vishik, I. M. *et al.* Phase competition in trisected superconducting dome. *Proc. Natl Acad. Sci. USA* **109,** 18332–18337 (2012).
6. Ino, A. *et al.* Electronic structure of $La_{2-x}Sr_xCuO_4$ in the vicinity of the superconductor–insulator transition. *Phys. Rev. B* **62,** 4137–4141 (2000).
7. Razzoli, E. *et al.* Evolution from a nodeless gap to $d^2_{x^2-y}$-wave in underdoped $La_{2-x}Sr_xCuO_4$. *Phys. Rev. Lett.* **110,** 047004 (2013).
8. Shen, K. M. *et al.* Fully gapped single-particle excitations in lightly doped cuprates. *Phys. Rev. B* **69,** 054503 (2004).
9. Drachuck, G. *et al.* Comprehensive study of the spin-charge interplay in antiferromagnetic $La_2Sr_xCuO_4$. *Nature Commun.* **5,** 3390 (2014).
10. Volovik, G. E. *The Universe in a Helium Droplet* (The International Series of Monographs on Physics, Book 117, Oxford Univ. Press, 2003).
11. Horava, P. Stability of Fermi surfaces and K theory. *Phys. Rev. Lett.* **95,** 016405 (2005).
12. Wang, F. & Lee, D-H. Topological relation between bulk gap nodes and surface bound states: Application to iron-based superconductors. *Phys. Rev. B* **86,** 094512 (2012).
13. Matsuura, S., Chang, P-Y., Schnyder, A. P. & Ryu, S. Protected boundary states in gapless topological phases. *J. Phys.* **15,** 065001 (2013).
14. Fujita, K. *et al.* Spectroscopic imaging scanning tunneling microscopy studies of electronic structure in the superconducting and pseudogap phases of cuprate high-T_c superconductors. *J. Phys. Soc. Japan* **81,** 011005 (2012).
15. Chen, W., Khaliullin, G. & Sushkov, O. P. Coulomb disorder effects on angle-resolved photoemission and nuclear quadrupole resonance spectra in cuprates. *Phys. Rev. B* **80,** 094519 (2009).
16. Schnyder, A. P., Ryu, S., Furusaki, A. & Ludwig, A. W. W. Classification of topological insulators and superconductors in three spatial dimensions. *Phys. Rev. B* **78,** 195125 (2008).
17. Kitaev, A. Periodic table for topological insulators and superconductors. *AIP Conf. Proc.* **1134,** 22–30 (2009).
18. Davis, J. C. S. & Lee, D-H. Concepts relating magnetic interactions, intertwined electronic orders, and strongly correlated superconductivity. *Proc. Natl Acad. Sci. USA* **110,** 17623–17630 (2013).
19. Wen, X-G. Symmetry-protected topological phases in noninteracting fermion systems. *Phys. Rev. B* **85,** 085103 (2012).
20. Altland, A. & Zirnbauer, M. R. Nonstandard symmetry classes in mesoscopic normal-superconducting hybrid structures. *Phys. Rev. B* **55,** 1142–1161 (1997).

Acknowledgements

We thank Y. He and M. Hashimoto for useful discussions. We especially thank J. Xia for pointing out to us that Kerr rotation is a candidate experiment to probe the chiral nature of the proposed SC state. This work was supported by the US Department of Energy, Office of Science, Basic Energy Sciences, Materials Sciences and Engineering Division, grant DE-AC02-05CH11231 (Y-M.L., D-H.L.).

Author contributions

Y-M.L. completed the symmetry/topological classification. T.X. proposed studying the 'nodal gap' phenomenon. D-H.L. designed the research, performed the effective theory calculation and partially carried out the symmetry/topological classification.

Additional information

Supplementary information is available in the online version of the paper. Reprints and permissions information is available online at www.nature.com/reprints. Correspondence and requests for materials should be addressed to D-H.L.

Competing financial interests

The authors declare no competing financial interests.

© 2014 Macmillan Publishers Limited. All rights reserved